Journal of Solid Mechanics and Materials Engineering

Vol. 2, No. 4, 2008

Absolute Fringe Order Determination in Digital Photoelasticity*

Pichet PINIT** and Eisaku UMEZAKI***

**King Mongkut's University of Technology Thonburi

126 Prachautid, Bangmod, Thungkru, Bangkok 10140, Thailand

E-mail: ipichet@yahoo.com

*** Nippon Institute of Technology

4-1 Gakuendai, Miyashiro, Saitama 345-8501, Japan

E-mail: umezaki@nit.ac.jp

Abstract

An improvement of the already proposed phase unwrapping algorithm for directly processing the triangular-typed wrapped phase map of the isochromatic parameter, photoelastically generated by an arccosine function based on the well-known technique of phase-shifting, is presented. In phase unwrapping algorithm, at any pixel, a three-dimensional plane and its normal vector are generated using three fractional (relative) fringe order values. Its generated plane is then adjusted using the orthogonal projection associated with the reference plane. Such point is unwrapped on the basis of regularization. The quality guide map is used to guide phase unwrapping and to mask out the conflictive regions such that they are lastly processed. The circular disk under compression demonstrated the performance of the improved algorithm. Results showed the accuracy improvement in such conflictive regions with reasonable agreement to theory.

Key words: Absolute Fringe Order, Digital Photoelasticity, Fractional Fringe Order

1. Introduction

The isochromatic parameter, δ, is one of the important parameters in the field of photoelasticity. A number of methods based on the phase-shifting technique (PST) have been proposed [(1)-(9)] to evaluate it. Those methods used the circular [(1)-(3)], semi-circular [(4)] or plane [(5)-(9)] polariscope system. As well known, the circular polariscope and semicircular polariscope based methods provides the fractional fringe order in the form of a saw tooth type through the arctangent operator. This type of wrapped phase map is thus simple for the phase unwrapping (PU) algorithm to render the absolute fringe order. Good results were given by them based on the significant condition that the isoclinic parameter must be first expressed in its true phase interval, $-\pi/2$ to $+\pi/2$. If this is not fulfilled, unwrapping the isochromatic parameter is impossible except for the work done by Sai Prasad et al. [(10)] in which the ambiguous zones in the wrapped phase map of δ were manually corrected before unwrapping. Manual correction is, however, very tedious task. Apart from such condition, the results obtained might be affected by the mismatch error of the quarter-wave plate used.

For those methods based on the use of the plane polariscope [(5)-(9)], the wrapped phase map obtained is of a triangular type due to the use of arccosine operator. In this case, the unwrapping process is difficult because the wrapped phase map possesses the sign ambiguity due to the nature of the cosine function (even function). Chen [(2)], Sarma et al. [(5)] and Plouzennec et al. [(8)-(9)] had attempted to directly unwrap this type of wrapped phase map. Chen's and Sarma et al's methods used the unload fringe pattern which limited the methods to the frozen slices. The Plouzennec et al's methods provide good results if there is

*Received 16 Nov., 2007 (No. 07-0727)
[DOI: 10.1299/jmmp.2.519]

zero-order fringe in the fringe field.

The present authors have been recently presented the new phase unwrapping working directly with the triangular type wrapped phase map with the concept of the three-dimensional (3D) plane generated from the fractional fringe order [11]. The performance of such proposed method was theoretically examined with the limitation at and near the conflictive regions, the load application and reaction points. This work is then to improve the performance of the proposed PU algorithm at such zones. The performance of the proposed method is theoretically examined with the problem of the circular disk under compressive load.

2. Determination of Fringe Order

2.1 Equation of fractional fringe order

The equations of fractional retardation, $\delta_\lambda^{\mathrm{f}}$, and fringe order, N_λ^{f}, can be written, respectively, as [11]

$$\delta_\lambda^{\mathrm{f}} = \cos^{-1}\left(1 - \frac{2I_{\mathrm{mod},\lambda}}{I_{\mathrm{p},\lambda}}\right) \quad \text{for} \quad I_{\mathrm{mod},\lambda} \le I_{\mathrm{p},\lambda} \tag{1}$$

and

$$N_\lambda^{\mathrm{f}} = \frac{1}{2\pi}\cos^{-1}\left(1 - \frac{2I_{\mathrm{mod},\lambda}}{I_{\mathrm{p},\lambda}}\right) \quad \text{for} \quad I_{\mathrm{mod},\lambda} \le I_{\mathrm{p},\lambda} \tag{2}$$

where λ is wavelength of the light source, $I_{\mathrm{mod},\lambda}$ and $I_{\mathrm{p},\lambda}$ are the modulated intensity and the intensity coming out of the polariscope at the given wavelength λ. The superscript 'f' only denotes that these parameters are of fractional or relative value. Equations (1) and (2) are mathematically limited in the range 0 to π, and 0 to 0.5, respectively, due to the range of the arccosine function.

The relation between $\delta_\lambda^{\mathrm{f}}$ and N_λ^{f} is given by [11]

$$\frac{\delta_\lambda^{\mathrm{f}}}{2\pi} = N_\lambda^{\mathrm{f}} = \frac{C_\lambda h}{\lambda}(\sigma_1 - \sigma_2) = \frac{h}{f_{\sigma,\lambda}}(\sigma_1 - \sigma_2) \tag{3}$$

where C_λ is the stress-optic coefficient, $f_{\sigma,\lambda}$ (= λ / C_λ) is the material stress fringe value obtained by calibration and h is the thickness of the model studied.

2.2 Equation of absolute fringe order

Due to the multiple-valued function of the trigonometric function, the absolute fringe order N_λ^{u} can be written as [11]

$$N_\lambda^{\mathrm{u}} = N_{\mathrm{int}} \pm N_\lambda^{\mathrm{f}} \quad \text{for} \quad N_\lambda^{\mathrm{u}} \ge 0 \quad \text{and} \quad N_{\mathrm{int}} \ge 0 \tag{4}$$

The superscript 'u' denotes the absolute fringe value or unwrapped value and N_{int} is an integral fringe value. The upper and lower signs are used when N_{int} = 0, 1, 2, … and N_{int} = 1, 2, 3, …, respectively.

Since the state of stress at the same point on the model is the same for different wavelengths [2]; hence, from Eq. (3), the following relation is valid.

$$N_\lambda^{\mathrm{u}} f_{\sigma,\lambda} = h(\sigma_1 - \sigma_2) = K \tag{5}$$

where K is a constant. Then, for three RGB wavelengths used here, Eq. (5) can be rewritten as

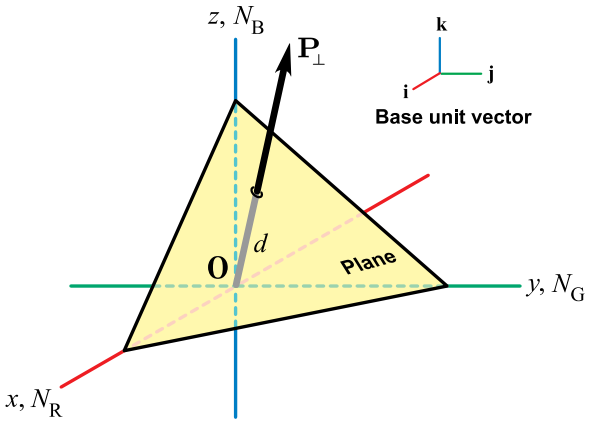

Fig. 1 Three-dimensional (3D) plane and vector $\mathbf{P}_\perp$ normal to the plane generated in the fringe order space that is analogous to the Cartesian coordinates as shown.

$$N_{\mathrm{R}}^{\mathrm{u}} f_{\sigma,\mathrm{R}} = N_{\mathrm{G}}^{\mathrm{u}} f_{\sigma,\mathrm{G}} = N_{\mathrm{B}}^{\mathrm{u}} f_{\sigma,\mathrm{B}} = h(\sigma_1 - \sigma_2) = K \tag{6}$$

Equation (6) is used later for the generation of the 3D reference plane which acts as a plane calibrator for the detection of the seed point.

3. Phase Unwrapping (PU)

3.1 Three-dimensional plane

Consider the fringe order space as shown in Fig. 1. Note the way that this fringe order space is analogous to the Cartesian coordinates. The coordinates of the points at the intersection between the plane and the axes are, respectively, (N_{R}, 0, 0), (0, N_{G}, 0) and (0, 0, N_{B}). Then, by these three points, the vector normal to the plane is given as [11]

$$\mathbf{P}_\perp = N_{\mathrm{G}} N_{\mathrm{B}} \mathbf{i} + N_{\mathrm{R}} N_{\mathrm{B}} \mathbf{j} + N_{\mathrm{R}} N_{\mathrm{G}} \mathbf{k} \tag{7}$$

and its unit vector

$$\mathbf{n}_\perp = \frac{\mathbf{P}_\perp}{|\mathbf{P}_\perp|} \tag{8}$$

The unit vector is used for detection of the seed point. It should be noted that, by the nature of the fringe order ($N_\lambda > 0$) and Eq. (6), the generated 3D plane is only in the first octant and $\mathbf{P}_\perp$ or $\mathbf{n}_\perp$ always points outwards from the origin O and their direction is totally constant. When all absolute fringe order becomes zero, there is no such plane (the plane turns to be a point) and $\mathbf{P}_\perp$ is a null vector.

3.2 Quality map

As shown in the work proposed in Ref. (11), the simulated unwrapped phase map of N_λ obtained from the wrapped phase map (Fig. 2a) was greatly comparable to that of theory except for the region at and near the load application point (see Figs. 2b and its magnification in Figs. 2c and 2d).

The quantity used to guide the PU algorithm was the values of $I_{\mathrm{mod,avg}} = \frac{1}{3}(I_{\mathrm{mod,R}} + I_{\mathrm{mod,G}} + I_{\mathrm{mod,B}})$. $I_{\mathrm{mod,avg}}$ values can be thought as a quality indicator for the pixel of interest.

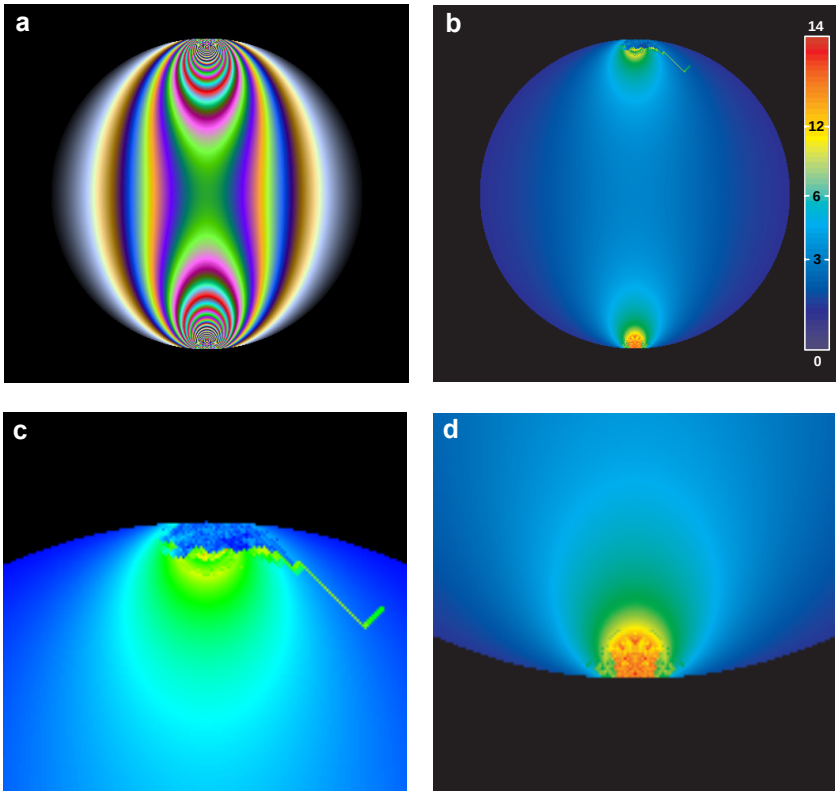

Fig. 2 Wrapped (fractional) and unwrapped (absolute) fringe order maps: (a) wrapped map (superposition of $N_{\mathrm{R}}^{\mathrm{f}}$, $N_{\mathrm{G}}^{\mathrm{f}}$, and $N_{\mathrm{B}}^{\mathrm{f}}$), (b) unwrapped map of $N_{\mathrm{G}}^{\mathrm{u}}$ (shown in this color scale for the sake of clarity), (c) close-up view of upper portion around the load application point in (b), and (d) close-up view of lower portion around the reaction point in (b). The unwrapped map in (b) was obtained from the PU algorithm proposed in Ref. (11). The size of (a) and (b) is of 512 × 480 pixels.

The quality maps are the arrays of the values of quality indicator indicating the goodness (or badness) of the phase data of all points in the fringe field. For simplicity, the values generally are normalized into the range from 0 to 1 by which one represents the best quality and zero shows the lowest quality.

The reason why the errors occurred at and near the load application has been explained in Ref. (11); however, for clarity, it should be mentioned here. That is, at and near the load application point, the fringe undulation changes rapidly; hence, the use of any pixel in such region to be the seed point for unwrapping causes the error propagation to neighboring pixels. Figure 2c shows this error propagation. It is evident that only the use of $I_{\mathrm{mod,avg}}$ to guide the PU algorithm leads to wrong unwrapped values. Then, to solve this problem, such regions (both upper and lower parts) have to be masked out and to be lastly processed by the PU algorithm. Other quality maps used to fulfill such need are the pseudo-correlation and phase derivative variance [12].

3.2.1 Pseudo-correlation map (PCM)

The quality of any pixel by the pseudo-correlation map is given by

$$Q_{m,n} = \frac{\sqrt{(\sum \sin \delta_{i,j})^2 + (\sum \cos \delta_{i,j})^2}}{k^2} \tag{9}$$

where $Q_{m,n}$ represents the quality of the central pixel at location m and n of the square $k \times k$

kernel where k is the number of pixel. The summation in Eq. (9) is performed over all pixel inside the kernel. $\delta_{i,j}$ is the fractional retardation at location i and j inside such kernel and can be obtained from Eq. (1).

3.2.2 Phase derivative variance map (PDVM)

The quality of any pixel by the phase derivative variance map is given by

$$Q_{m,n} = -\frac{\sqrt{\sum(\Delta^x_{i,j} - \bar{\Delta}^x_{m,n})^2 + \sum(\Delta^y_{i,j} - \bar{\Delta}^y_{m,n})^2}}{k^2} \tag{10}$$

where $Q_{m,n}$ denotes the quality of the central pixel at location m and n of the same $k \times k$ kernel as described for Eq. (9). The terms $\Delta^x_{i,j}$ and $\Delta^y_{i,j}$ are the partial derivatives of the wrapped retardation $\delta_{i,j}$ at location i and j determined by the two-point forward finite difference. The terms $\bar{\Delta}^x_{m,n}$ and $\bar{\Delta}^y_{m,n}$ are the average of these partial derivatives in such kernel.

3.3 Procedure of PU

The improved PU algorithm involves the following steps:

Step 1: Compute the fractional fringe values for each wavelength using Eq. (2).

Step 2: Generate a reference plane by means of the vector normal to the plane using Eq. (7). That is, let $N_R = N^u_R$ by which the values of N^u_R (or N^u_G, N^u_B) is assumed to be known and of $f_{\sigma,\lambda}$ are obtained from the calibration, yields [11]

$$\mathbf{P}^{ref}_{\perp} = N^u_G N^u_B \mathbf{i} + N^u_R N^u_B \mathbf{j} + N^u_R N^u_G \mathbf{k} \tag{11}$$

Due to the validity of Eq. (6), all vectors for all pixels in the domain are collinear after unwrapping.

Step 3: Detect points or pixels whose fractional fringe order values satisfying the following conditions: [11]

- $N^f_R < N^f_G < N^f_B$ and
- $N^f_R \geq 0.1$ and $N^f_B \leq 0.4$

The first condition comes from the implication of Eq. (6) for which the zero-fringe order is discarded. The second condition is to prevent the use of unreliable fractional fringe values because, generally, the fractional fringe values does neither start from 0 nor end with 0.5 (this range is dependent of the user but $N^f_R > 0$).

Step 4: Detect the seed point using the vectorial matching. For all pixels detected from step 3, use each set of those three fringe order values to generate the vector normal to the plane and then its unit vector ($\mathbf{P}_{\perp}$ and $\mathbf{n}_{\perp}$). Then, the pixel in a largest region (group of pixels) which possesses a maximum of $\mathbf{n}^{ref}_{\perp} \cdot \mathbf{n}_{\perp}$ (vector dot product) is chosen to be the seed point for unwrapping. Note that the pixel possessing $\mathbf{n}^{ref}_{\perp} \cdot \mathbf{n}_{\perp} \geq 0.8$ is considered in order to speed up the process. Generally, the generated plane at this seed point is not parallel to the reference plane $\mathbf{P}^{ref}_{\perp}$ obtained from step 2; hence, in order to make them parallel, the orthogonal projection can be applied. By doing this, the very accurate values of the absolute fringe orders at the seed pixel can be obtained.

Step 5: Compute the pseudo-correlation or the phase derivative variance map using Eq. (9) or (11). Let T_{cut} be a predefined threshold determined by a user. For any pixel in the fringe field, if $Q \leq T_{cut}$, it is considered to be a bad pixel and, then, it is masked out in order that it is lastly unwrapped. However, since at such conflictive regions, the fringe density is problematically very high, the value of Q may be not uniform for the neighboring pixels; therefore, it is better to expand such cut pixel to be a region. Then, let $\Gamma_{w \times h}$ be a kernel for

this expansion where w and h are the width and height, respectively. Therefore, by properly selecting values of w and h, the unreliable regions at and near the load application and reaction points are marked or cut out.

Step 6: Perform unwrapping starting from the seed pixel (also seed plane) obtained from step 4 with the regularization [13]. The seed pixel is used as the central pixel of the 8-neighbors mask window. Then, for the wrapped pixels locating inside the mask window, minimize [11]

$$E = \min_{d,N_\lambda^{\mathrm{u}}} \left\{ [d - d_{\mathrm{c}}]^2 + \sum_{\lambda} [I_\lambda - \cos(2\pi N_\lambda^{\mathrm{u}})]^2 \right\} \tag{12}$$

where d (≥ 0) is the shortest distance from the generated plane to the origin of the coordinates of the pixel being considered and d_{c} is also the shortest distance but of the central pixel. $I_\lambda (= \cos \delta_\lambda^{\mathrm{f}})$ can be obtained from Eq. (1). It should be noted that, in term of d, the generated plane of the considered pixel is automatically parallel to the reference plane and also $\mathbf{n}_\perp = \mathbf{n}_\perp^{\mathrm{ref}}$. Then, the absolute fringe order in term of d can be written as

$$N_\lambda^{\mathrm{u}} = \frac{d}{n_{\perp,\lambda}} = \frac{d}{n_{\perp,\lambda}^{\mathrm{ref}}} \tag{13}$$

Note that, $n_{\perp,\lambda}^{\mathrm{ref}}$ (or $n_{\perp,\lambda}$) is the directional cosine of the unit vector with respect to the Cartesian coordinates or fringe order space (Fig. 1). Therefore, the merit functional to be minimized can be rewritten as

$$E = \min_{d} \left\{ [d - d_{\mathrm{c}}]^2 + \sum_{\lambda} [I_\lambda - \cos(2\pi \tfrac{d}{n_{\perp,\lambda}^{\mathrm{ref}}})]^2 \right\} \tag{14}$$

For the pixel being considered, define $(d_{\mathrm{c}} + 1) \leq d \leq (d_{\mathrm{c}} - 1)$ where $(d_{\mathrm{c}} + 1)$ and $(d_{\mathrm{c}} - 1)$ are the upper and lower bounds of the shortest distance set, respectively. Then, by reducing d value with the known step $s = 1/10^k$, where k (= 0, 1, 2, . . .) is the iteration number, from the upper bound to the lower one and computing E at each step, yield the minimum E and the associated d. E value and its associated d value are registered into an array.

For the next $(k + 1)$th round iteration, d values at the array indexes former and later the index pointing to the minimum E at the kth round iteration are reassigned to be the upper and lower bounds of the $(k + 1)$th iteration. The process is repeated until the difference between these bounds satisfies a predefined stopping criterion. After stopping, the absolute fringe orders for each wavelength are obtained from Eq. (14). It should be noted that the unwrapping order for the wrapped pixels in the 8-neighbors mask window is controlled by the value of $I_{\mathrm{mod,avg}}$, i.e., pixel having the maximum $I_{\mathrm{mod,avg}}$ is unwrapped first and the pixel with the minimum $I_{\mathrm{mod,avg}}$ is lastly unwrapped. As clearly seen in Fig. 2 that only the use of $I_{\mathrm{mod,avg}}$ to guide the PU algorithm leads to wrong unwrapped values. Then, in stead of using $I_{\mathrm{mod,avg}}$, the pseudo-correlation or the phase derivative variance quality maps can also be employed. This process is repeated until all pixels in the domain are unwrapped.

For clarity, the whole process of the PU algorithm is divided into two stages: an expansion stage and a shrinkage stage. The expansion stage handles all points that are not masked out in step 5. That is, the PU algorithm starting from the seed point and the unwrapped region continuously grows from its outer most boundaries. For the shrinkage stage, the pixels in the masked region are unwrapped and such region gradually become smaller from the outer most boundaries. Both stages are guided by the quality map. It is to be noted again that before the expansion stage taking place, the quality map masks out the conflictive regions.

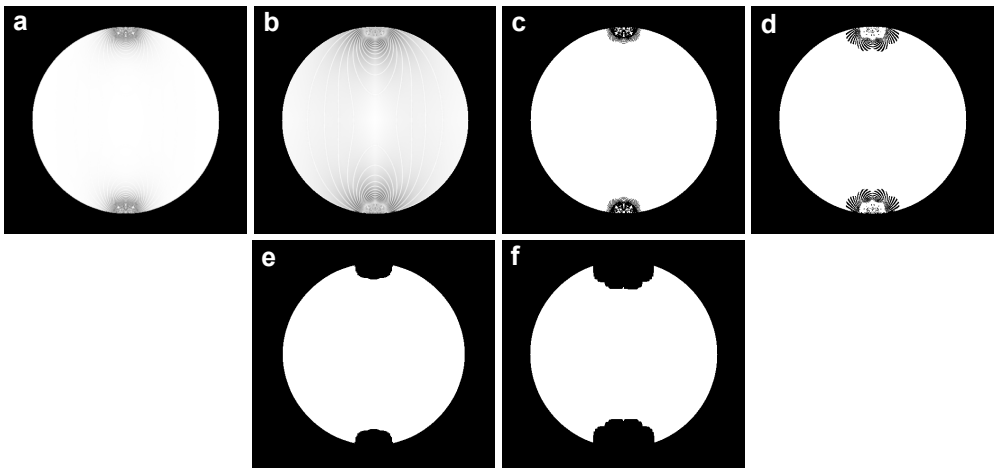

Fig. 3 Quality guide maps and their mask images: (a) pseudo-correlation quality map, (b) phase derivative variance quality map, (c) mask image of (a), (d) mask image of (b), (e) expanded masked region of (c), and (f) expanded masked regions of (d). These images were obtained from step 5 in section 3.3.

4. Numerical Simulation

4.1 Conditions for simulation

The circular disk subjected to diametral compressive load was also used as in Ref. (11) in order of comparison. The diameter and thickness of circular disk model were of 30 mm and 6 mm, respectively. The material stress fringe values used to simulate the fringe patterns were $f_{\sigma,\mathrm{R}}$ = 11.20, $f_{\sigma,\mathrm{G}}$ = 10.01 and $f_{\sigma,\mathrm{B}}$ = 7.997 N/(mm·fringe). They were of epoxy resin plate and calibrated at wavelengths R = 612 nm, G = 547 nm and B = 437 nm. When simulating, the disk was virtually loaded by a force P of 274 N. The photoelastic fringe patterns were generated based upon the equation in Ref. (14). The stopping criterion (the difference between the upper and lower bounds), which is the user dependent parameter, was set to be 1×10^{-5}. With those material fringe values, the reference vector $\mathbf{P}_{\perp}^{\mathrm{ref}}$ normal to the reference plane can be determined. That is, by assuming $N_{\mathrm{G}}^{\mathrm{u}} = 1.000$, with Eqs. (6) and (12), yields $N_{\mathrm{R}}^{\mathrm{u}} = 0.8940$ and $N_{\mathrm{B}}^{\mathrm{u}} = 1.252$ and, then, using Eqs. (7) and (8), also yields $\mathbf{P}_{\perp}^{\mathrm{ref}} = 1.252\mathbf{i} + 1.119\mathbf{j} + 0.8940\mathbf{k}$ and $\mathbf{n}_{\perp}^{\mathrm{ref}} = 0.6581\mathbf{i} + 0.5882\mathbf{j} + 0.4670\mathbf{k}$. Note that $\mathbf{P}_{\perp}^{\mathrm{ref}}$ is obtained from Eq. (6); therefore, other planes that are parallelly derived from this reference plane do perfectly satisfy Eq. (6). This is also true for $N_{\mathrm{R}}^{\mathrm{u}}$, $N_{\mathrm{G}}^{\mathrm{u}}$, and $N_{\mathrm{B}}^{\mathrm{u}}$ for the point being considered. Further, after completing unwrapping process, all vectors in the fringe field are collinear.

It is instructive to note that whatever the value of $N_{\mathrm{G}}^{\mathrm{u}}$ is, $\mathbf{n}_{\perp}^{\mathrm{ref}}$ is still the same, even though $\mathbf{P}_{\perp}^{\mathrm{ref}}$ has different values. This means that there are infinite 3D planes associated with $\mathbf{P}_{\perp}^{\mathrm{ref}}$ in the fringe order space (Fig. 1) and this implies the name 'hyperplane' phase unwrapping. One of these reference planes can be used as the plane calibrator.

4.2 Results of simulation

Figure 2a shows the wrapped fractional fringe map which was computationally obtained using Eq. (2) with the simulated images. The continuous unwrapped phase map of $N_{\mathrm{G}}^{\mathrm{u}}$ as shown in Fig. 2b was rendered from the original PU algorithm [11]. Note that for the map of the wrapped retardation $\delta_{\mathrm{G}}^{\mathrm{f}}$, it is identical to Fig. 2a but the values are different (see Eq. (3)).

Figure 3 displays the quality guide maps and their mask images of the conflictive regions at and near the load application and the reaction points. Figures 3a and 3b were

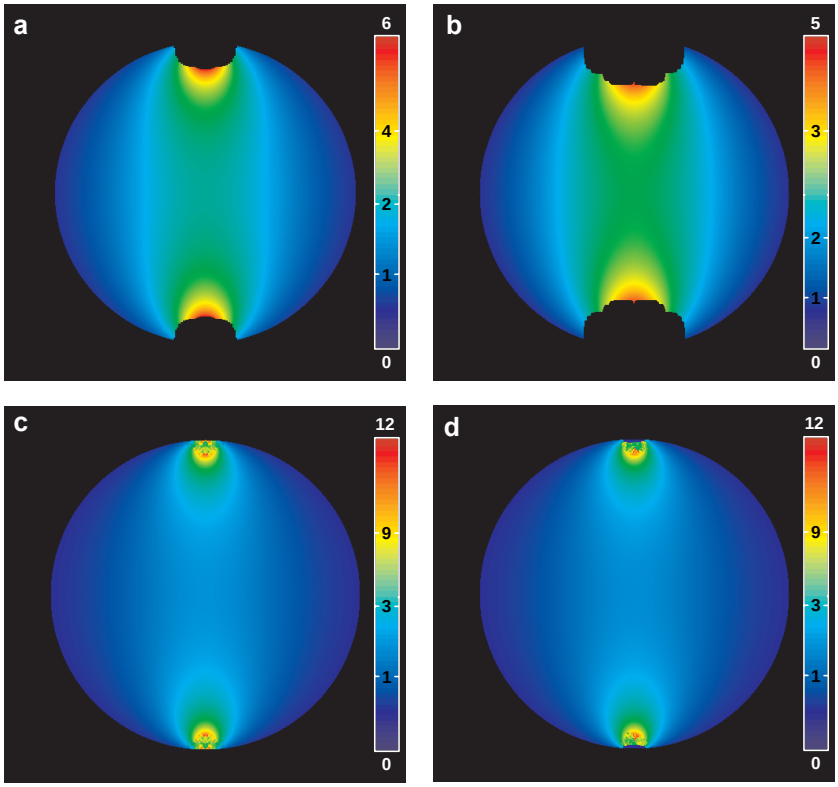

Fig. 4 Unwrapped absolute fringe order map of $N_{\mathrm{G}}^{\mathrm{u}}$ obtained from the expansion and shrinkage stages: (a) unwrapped absolute fringe order map obtained using the pseudo-correlation quality map in Fig. 3a and the mask image in Fig. 3e (expansion stage), (b) unwrapped absolute fringe order map obtained using the phase derivative variance quality map in Fig. 3b and the mask image in Fig. 3f (expansion stage), (c) complete unwrapped absolute fringe order map after performing shrinkage stage of (a), and (d) complete unwrapped absolute fringe order map after performing shrinkage stage of (b).

obtained using $\delta_{\mathrm{G}}^{\mathrm{f}}$ with a 3 × 3 kernel (k = 3). The quality values were normalized into the range 0 to 1 by which 0 represents deep black and 1 represents pure white. With T_{cut} = 0.7, Figs. 3c and d were given and Figs. 3e and 3f were, respectively, provided from Figs. 3c and 3d with $\Gamma_{9\times9}$ and $\Gamma_{17\times17}$. Note that the two parameters, T_{cut} and $\Gamma_{w\times h}$, are user-dependent. The reason why those quality maps were determined for only $\delta_{\mathrm{G}}^{\mathrm{f}}$ is that the proposed algorithm used the material fringe value $f_{\sigma,\lambda}$ to help the 3D plane generation and $f_{\sigma,\lambda}$ can be obtained from the calibration according to the wavelengths used. It is evident that only $f_{\sigma,\mathrm{G}}$ which is experimentally obtained is very close to the theoretical value [15]. Therefore, the green channel of the fringe image can be considered to be equivalent to the image recorded by a green filter. Then, the determination of quality maps could gain a benefit from $\delta_{\mathrm{G}}^{\mathrm{f}}$. This also discloses the derivation method for finding $\mathbf{P}_{\perp}^{\mathrm{ref}}$.

Figure 4 shows the continuous unwrapped absolute fringe order map. The unwrapped maps provided from the expansion stage are shown in Figs. 4a and 4b for the pseudo-correlation and the phase derivative variance, respectively. Note that, at this expansion stage, $I_{\mathrm{mod,avg}}$ can be used to guide the PU algorithm and the unwrapped map obtained was identical to Fig. 4a or 4b (see Fig. 2b and note that their actual unwrapped fringe order values were similar). After executing the shrinkage stage, the unwrapped maps obtained are depicted in Figs. 4c and 4d corresponding to Figs. 4a and 4b. Topographical maps of the unwrapped maps as shown in Figs. 2b and 4c are respectively depicted in Figs. 5a and 5b and they are displayed only in the y-z view.

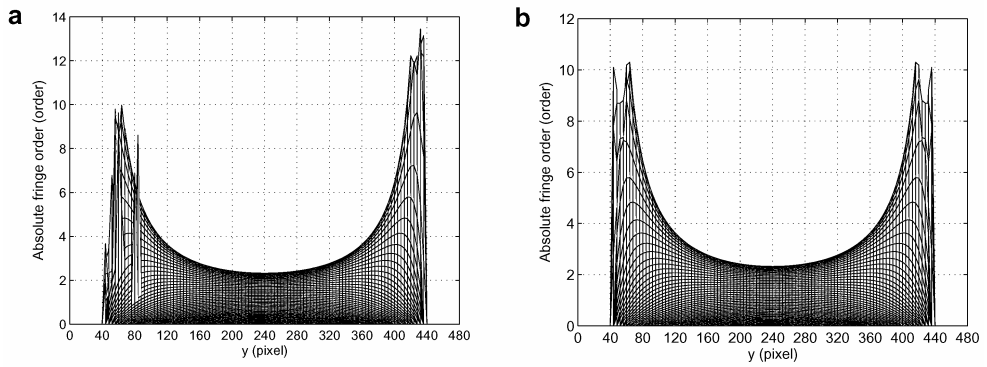

Fig. 5 Topographical maps of the unwrapped absolute fringe order map of N_G^u shown only the *y*-*z* view in the image coordinates: (a) map of Fig. 2b obtained from the method proposed in Ref. (11) and (b) map of Fig. 3c obtained from expansion and shrinkage stages of the proposed method. The step used to plot these topographical maps was 4 pixels for both *x* and *y* directions. The *z*-axis is coincident to the axis of the absolute fringe order.

5. Discussion

As obviously seen in Fig. 2c that the unwrapped absolute fringe order values obtained at and near the load application and reaction points contain errors. $I_{mod,avg}$ itself is the good quality indicator for guiding the PU algorithm to unwrap all points in the field of view but its rapid undulation at the conflictive regions degraded its guidance performance. To handle this problem, then, such regions have to be excluded or masked out.

Since, $I_{mod,avg}$ is derived directly from the intensity, it, then, cannot be used to be as a conflictive-point masker because, if it is used, other pixels locating further away from such erroneous regions may also be masked out. For the masker, other quality maps can be employed. The widely used quality map is the pseudo-correlation map and the phase derivative variance map [12]. Note that the required quality map must have ability for identifying the conflictive points or regions. Comparing Fig. 3c to Fig. 3d, reveals that the ability for conflictive-point detection of the pseudo-correlation is better than that of the phase derivative variance. It is seen that the unwrapped maps rendered from the PU algorithm with different quality maps are almost identical (Figs. 4c and 4d). The errors that might happen and propagate to the neighboring pixels were confined within the conflictive regions. This shows the improvement of the proposed PU algorithm (compare with Fig. 2b).

It is seen that the fringe order value at the right lobe of Fig. 5a is higher than that of Fig. 5b; however, at the left lobe of Fig. 5a, the errors (see Fig. 2c) expressed themselves considerably whereas Fig. 5b contains no such errors and reflects accurately the physical situation of the problem; that is, the left and right lobes should have similar fringe order values. It should be noted that the maximum scales used in Fig. 5 are different from those used in Figs. 4c and 4d. In Figs. 4c and 4d, the maximum fringe order values expressed themselves as outlier data; hence, they were discarded but in Fig. 5, actual data were used to plot the maps.

The difference in the ability of the two quality guide maps used should be addressed here. Generally the phase derivative variance map is the most reliable measure of phase quality [12]. Nevertheless, by its nature, it cannot be responsive to the regions of high-phase variation. Since, for the problems in the photoelasticity, there always exist the high-phase variation regions (region at and near the load application and reaction points) due to the applied load; hence, the phase derivative variance failed to identify them. In case of the pseudo-correlation, it can greatly recognize the regions of high-phase variation; however, it may have error coming up with the use of it.

Close inspection of Figs. 3a and 3b for those regions corresponding to the white regions in the mask images shown in Figs. 3e and 3f, reveals that the quality values are different. The pseudo-correlation provided almost equal quality values for such region, i.e., assigning the high quality value for the most pixels, while the phase derivative variance graded considerably different qualities. This is important because when unwrapping with the pseudo-correlation quality map, this difference is over looked and the low-quality pixel (but higher quality than the pixels in the conflictive regions) may be chosen to be the seed point. As a result, the error may happen and propagate to the neighboring pixels.

The obtained absolute fringe order values at the disk center from the PU algorithm were of 2.076, 2.323 and 2.908 for $N_{\mathrm{R}}^{\mathrm{u}}$, $N_{\mathrm{G}}^{\mathrm{u}}$, and $N_{\mathrm{B}}^{\mathrm{u}}$, respectively. For $N_{\mathrm{G}}^{\mathrm{u}}$, it can also be estimated from Fig. 5 (see at 240th pixel). The theoretical values of these absolute fringe order values can be calculated using the well-known equation [14]

$$\frac{4Pr}{\pi N_{\lambda}^{\mathrm{u}} f_{\sigma,\lambda}} = \frac{(r^2+x^2+y^2)^2 - 4r^2y^2}{r^2-x^2-y^2} \tag{15}$$

where P is the applied load, r is the radius of the disk, x and y are the typical axes in the Cartesian coordinates with the origin at the disk center. Then, by Eq. (15), at the central point ($x = y = 0$), $N_{\mathrm{R}}^{\mathrm{u}} = 2.0787$, $N_{\mathrm{G}}^{\mathrm{u}} = 2.3260$ and $N_{\mathrm{B}}^{\mathrm{u}} = 2.9112$. It is seen that the absolute fringe orders rendered from the PU algorithm are very close to these values, accordingly.

6. Conclusion

An improvement of the already proposed PU algorithm for an automatic determination of the absolute fringe order is presented. The method is theoretically examined by applying to the simulated photoelastic fringe images of the circular disk subjected to diametrically compressive load generated based on the four-step phase shifting technique.

With the cross-relation between the theoretical space (reference plane) and the experimental space (first seed plane), reliable unwrapped phase data is given. The obtained results show the significant improvement in the accuracy of the phase data in the conflictive region with the use of the quality map.

The use of the modulated intensity $I_{\mathrm{mod,avg}}$ to be the guidance provides the good profit of the highest absolute fringe order (Fig. 2b) but fails in the conflictive regions. Thus, the combination between these quality guide maps ($I_{\mathrm{mod,avg}}$, the pseudo-correlation quality map and the phase derivative variance map) may give another look of the quality guide map that is more suitable for solving the problems.

References

(1) Patterson, E.A. and Wang, Z.F., Strain, 27 (1991), pp. 49-56.
(2) Chen, T.Y., Exp. Mech, 37 (1997), pp. 232-236.
(3) Kihara, T., Strain, 39 (2003), pp. 65-71.
(4) Barone, S., Burriesci, G. and Petrucci, G., Exp. Mech, 42 (2002), pp. 132-139.
(5) Sarma, A.V.S.S.S.R., S.A.Pillai, G.S. and Varadan, T.K., Exp. Mech, 32 (1992), pp. 24-29.
(6) Buckberry, C. and Towers, D., Opt. Lasers Eng., 24 (1996), pp. 415-428.
(7) Nurse, A.D., Appl. Opt, 36 (1997), pp. 5781-5786.
(8) Plouzennec, N., Dupre, J.C. and Lagarde, A., Exp. Tech, 23 (1999), pp. 30-33.
(9) Plouzennec, N. and Lagarde, A., Exp. Mech, 39 (1999), pp. 274-277.
(10) Prasad, V.S., Madhu, K.R.K. R. and Ramesh, K., Opt. Lasers Eng, 42 (2004), pp. 421-436.

(11) Pinit, P., Nomura, Y. and Umezaki, E., Phase Unwrapping for Absolute Fringe Order in Photoelasticity, *Proceeding of the 13rd Int. Conf. on Experimental Mechanics* (ICEM13), (2007), on CD-ROM.
(12) Ghiglia, D.C. and Pritt, M.D., Two-dimensional Phase Unwrapping: Theory, Algorithm and Software, John Willey & Sons (1998), pp. 70-79.
(13) Quiroga, J.A. and Gonzalez-Cano, A., Appl. Opt, 39 (2000), pp. 2931-2940.
(14) Forcht, M.M., Photoelasticity, Vol. 2, John Willey & Sons (1967), p. 136.
(15) Ramesh, K. and Deshmukh, S.S., Opt. Lasers Eng, 28 (1997), pp. 47-60.